Whirling Modes and Parametric Instabilities in the Discrete Sine-Gordon Equation: Experimental Tests in Josephson Rings

Shinya Watanabe and Steven H. Strogatz*
Department of Mathematics, Massachusetts Institute of Technology, Cambridge, Massachusetts 02139

Herre S. J. van der Zant† and Terry P. Orlando
Department of Electrical Engineering and Computer Science, Massachusetts Institute of Technology, Cambridge, Massachusetts 02139

(Received 1 August 1994)

We analyze the damped driven discrete sine-Gordon equation. For underdamped, highly discrete systems, we show that whirling periodic solutions undergo parametric instabilities at certain drive strengths. The theory predicts novel resonant steps in the current-voltage characteristics of discrete Josephson rings, occurring in the return path of the subgap region. We have observed these steps experimentally in a ring of 8 underdamped junctions. An unusual prediction, verified experimentally, is that such steps occur even if there are no vortices in the ring. Numerical simulations indicate that complex spatiotemporal behavior occurs past the onset of instability.

PACS numbers: 05.45.+b, 03.20.+i, 74.40.+k, 74.50.+r

Many physical and biological systems may be regarded as collections of coupled nonlinear oscillators [1]. In particular, Josephson junction arrays have recently been studied from this point of view [2–6]. A one-dimensional parallel array of N identical junctions is governed by the damped, driven, discrete sine-Gordon equation:

$$\ddot{\phi}_j + \Gamma\dot{\phi}_j + \sin\phi_j = I + \Lambda^2(\phi_{j+1} - 2\phi_j + \phi_{j-1}), \tag{1}$$

for $j = 1,\ldots,N$. Here ϕ_j is the phase difference across the jth junction, Γ is the damping ($= \beta_c^{-1/2}$ with β_c the McCumber parameter), I is the drive (normalized dc bias current), and Λ is the coupling (normalized Josephson penetration depth). The dot denotes differentiation with respect to $\omega_p t$, where ω_p is the plasma frequency.

Equation (1) also arises in the Frenkel-Kontorova model of dislocations [7] and in models for ferroelectric and magnetic domain walls. A mechanical analog for (1) is a chain of N pendula, each of which is damped, driven by a constant torque, and coupled to its nearest neighbors by torsional springs. Despite its physical significance, not much is known about the dynamics of (1). The available studies suggest that the behavior can be extremely complicated, even for $N = 2$ pendula [8–10].

This Letter presents analytical and numerical studies of (1), for underdamped ($\Gamma < 1$), highly discrete ($\Lambda \leq 2$) systems. We also test our predictions experimentally, using a discrete ring of $N = 8$ Josephson junctions.

First we recall the properties of a single pendulum [11]. If we slowly increase the torque I from $I = 0$, the pendulum moves away from the downward vertical to a new static equilibrium angle $\phi = \sin^{-1} I$. When $I > 1$, the pendulum *whirls* according to some function $\phi = \phi^*(t)$, where $\phi^*(t + T) = \phi^*(t) + 2\pi$ and T is the rotation period. Let $V = \langle\dot{\phi}\rangle$ denote the time-averaged angular velocity [12]. Then V increases with I, for $I > 1$. Now suppose we decrease the torque. If the damping is sufficiently large, the pendulum will retrace its original I-V curve, becoming motionless as I approaches 1 from above. On the other hand, if the pendulum is sufficiently underdamped, the I-V curve exhibits hysteresis; because of inertia, the pendulum keeps whirling even if $I < 1$, until it finally stops at some value $I_r < 1$. Thus this "return portion" of the I-V curve approaches $V = 0$ as $I \to I_r$.

Next consider a ring of N pendula governed by (1). The ring geometry introduces a topological constraint,

$$\phi_{j+N} = \phi_j + 2\pi M, \tag{2}$$

where M is the number of twists or vortices trapped in the ring. [Without loss of generality, M can be restricted to $M = 0,\ldots,(N/2)$ due to a symmetry of Eqs. (1) and (2).] M is determined by the initial conditions, but it remains constant as the system evolves. We will see that the dynamics of (1) depend strongly on M.

The simplest case is $M = 0$. If $I < 1$, the system has a stable static solution with all the pendula in phase: $\phi_j = \sin^{-1} I$ for all j. However, for $I > 1$, the pendula start whirling; now the stability of the in-phase solution is less clear. To determine its stability, let $\phi_j(t) = \phi^*(t) + u_j(t)$, where $u_j(t)$ is a small perturbation. Then

$$\ddot{u}_j + \Gamma\dot{u}_j + [\cos\phi^*(t)]u_j = \Lambda^2\nabla^2 u_j, \tag{3}$$

where $\nabla^2 u_j = u_{j+1} - 2u_j + u_{j-1}$. The boundary conditions are periodic: $u_{j+N} = u_j$.

As long as I is not too close to I_r, the whirling solution may be approximated by $\phi^*(t) \approx \omega t$, where $\omega = 2\pi/T$. Expand $u_j(t)$ as a discrete Fourier series in space: $u_j(t) =$

0031-9007/95/74(3)/379(4)$06.00

$\sum_{m=0}^{N-1} A_m(t) \exp(2\pi i m j/N)$. Then the modes decouple:

$$\ddot{A}_m + \Gamma \dot{A}_m + [\omega_m^2 + \cos \omega t] A_m = 0, \qquad (4)$$

for $m = 0, \ldots, N-1$, where $\omega_m = 2\Lambda |\sin(m\pi/N)|$ is the lattice eigenfrequency of mode m.

Equation (4) is a damped Mathieu equation. It is known [13,14] that $A_m(t)$ grows exponentially for certain values of the parameters, in which case the in-phase whirling solution is *unstable* to the growth of mode m. In physical terms, the in-phase solution can destabilize itself by parametrically exciting the normal modes of the lattice, i.e., by exciting "phonons" [15].

These parametric instabilities occur only at certain rotation frequencies ω that resonate with the lattice eigenfrequencies, namely, $n\omega/2 \approx \omega_m$, where $n = 1, 2, \ldots$ is an index that labels the Mathieu tongues [13,14]. In our numerical experiments, we see only the $n = 1$ resonance: $\omega \approx 2\omega_m$ [16–18]. This resonance occurs for each $m = 0, \ldots, N-1$, but at most $N/2 + 1$ of these can be observed since $\omega_{N-m} = \omega_m$.

To test these predictions, we have measured the I-V characteristics of a ring of $N = 8$ niobium Josephson tunnel junctions. The parameters Λ and Γ can be measured and controlled experimentally. Moreover, the number of vortices in the ring can be controlled; when cooling down through the niobium transition temperature in a field of about M flux quanta applied to the ring, *exactly* M vortices will be trapped. Experimentally [6] we observed five distinct I-V curves (i.e., for $M = 0, \ldots, 4$); the I-V curve with $N - M$ trapped vortices is the same as that with M trapped vortices, consistent with the symmetry of the model. We also refer to [6] for more details about the sample and the experimental setup.

Figure 1 shows the I-V curve of a Josephson ring with $M = 0$ (no vortices in the ring). Starting from $I = 0$, the array remains in the superconducting state up to $I = 37\ \mu$A, where the jump to the steep gap region occurs. The upgoing part of the I-V is smooth, indicating that the whirling solution is stable. When I is decreased, there is hysteresis in the return path, and current steps occur at 0.93, 0.71, and 0.35 mV. As shown in Fig. 1, there is even hysteresis when biasing on these smaller steps.

The inset of Fig. 1 shows the voltage position of the steps as a function of the mode number m. The voltage is normalized to $V_0 = \Phi_0 \omega_0 / 2\pi$, where $\omega_0 = \Lambda \omega_p$ is a characteristic, temperature-independent frequency corresponding to the speed of light in the Josephson ring. As shown in [6], V_0 can be measured accurately and equals 0.25 mV for our ring. The solid line in the inset is the predicted resonance frequency $\omega = 2\omega_m$; no fitting parameters were used. We find close agreement between the data and our model.

So far, we have neglected the width of the Mathieu tongues. In fact, mode m is unstable for all ω in some interval $[\omega_-, \omega_+]$. For the tongue $n = 1$, perturbation theory [14,19] yields $\omega_+^2 \approx (4\omega_m^2 + 2)/(1 + \Gamma^2)$, valid for $1 \ll \omega < 1/\Gamma$. Numerical computation was used to check this formula, and to estimate ω_-. In Fig. 1 the intervals $[\omega_-, \omega_+]$ for $m = 1, \ldots, 4$ are shown as horizontal bars. The predicted intervals contain the observed steps, but they are smaller than the observed intervals. Also, the $m = 4$ step is missing in the experiment. We suspect that near the stability boundaries, thermal noise kicks the system out of the in-phase state prematurely.

Figure 2 is a numerically generated I-V curve for $N = 10$ junctions [20]. Four resonant steps, corresponding to $m = 1, \ldots, 4$, are resolved by sweeping I up and down several times. The predicted instability intervals for modes $m = 1, \ldots, 5$ are also shown. The intervals for $m = 4$ and 5 partially overlap, whereas the other intervals are separated by tiny gaps where the in-phase solution regains stability. At the right end of each interval, there is a sudden jump from the whirling solution to another attractor. In contrast, the bifurcation at the left end appears to be supercritical; a resonant step branches continuously from the in-phase solution [21].

The dynamics along a step can be complicated. As an example, we consider the $m = 3$ step of Fig. 2 at the

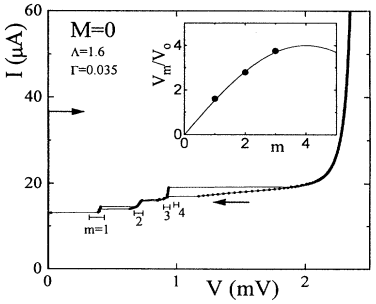

FIG. 1. Experimental I-V curve for $M = 0$ showing three resonant steps in the return path. The whirling in-phase solution is predicted to be unstable in the horizontal intervals. Inset: dots, measured voltage positions of the steps vs mode number m; solid curve, theoretical estimate $\omega = 2\omega_m$ (see text).

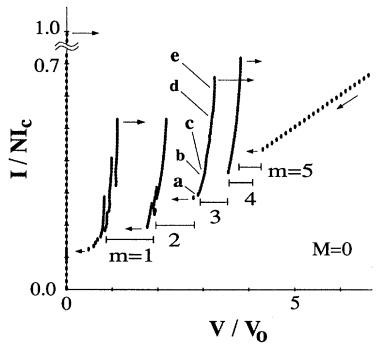

FIG. 2. Numerical I-V curve for (1) with $N = 10$, $M = 0$, $\Lambda^2 = 1$, $\Gamma = 0.1$. The in-phase solution is predicted to be unstable in the intervals $m = 1, \ldots, 5$. Attractors for a–e on the $m = 3$ step are shown in Figs. 3(a)–3(e), respectively.

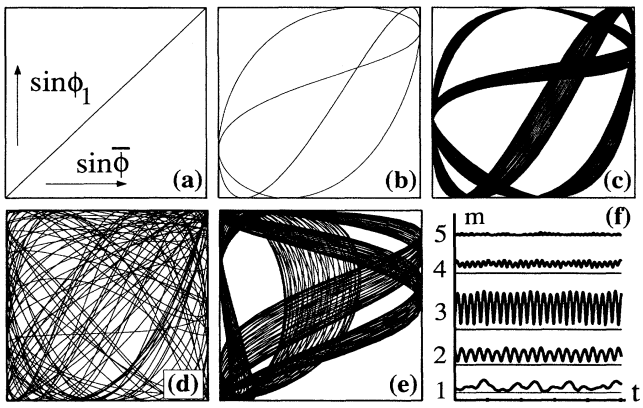

FIG. 3. (a)–(e) Phase portraits for the five points marked in Fig. 2, plotted in Lissajous-like representation. (a) $I = 0.29$, (b) $I = 0.35$, (c) $I = 0.365$, (d) $I = 0.53$, (e) $I = 0.62$, and (f) time series of spatial Fourier amplitudes $|A_m(t)|$ for (d).

points marked "a" through "e." Figure 3(a)–3(e) plots $\sin\phi_1(t)$ versus $\sin\bar{\phi}(t)$, where $\bar{\phi} = \sum_{j=1}^{N}\phi_j/N$. Figure 3(a) shows the stable in-phase solution. The corresponding point a in Fig. 2 is in the tiny gap between the $m = 2$ and $m = 3$ intervals. As I is increased, the solution period doubles [Fig.3(b)] as expected from Mathieu theory [13,14], but then it does *not* follow a period-doubling route to chaos. Instead we see a secondary Hopf bifurcation to a 2-torus [Fig. 3(c)], transition to an irregular motion [Fig. 3(d)], reversion to a 2-torus [Fig. 3(e)], collapse to a different period-doubled limit cycle (not shown), and a jump back to the in-phase whirling solution at $I \approx 0.67NI_c$ (Fig. 2).

The irregular state corresponding to Fig. 3(d) is also spatially complex. Figure 3(f) shows the magnitude $|A_m(t)|$ of spatial modes $m = 1,\ldots,5$. The mode $m = 3$ is the most active since the system is on the $m = 3$ step. The mode $m = 1$ seems to fluctuate aperiodically.

We have studied the dynamics on the other steps and found both generic and step-dependent features. Generically, the dynamics become simple (either periodic or quasiperiodic with two frequencies) near the onset *and* near the top of the steps. Near the onset, the solution is approximately in phase, with a small-amplitude mth mode superimposed. Near the top of a step, the fluctuation amplitude becomes large. The dynamics here can be described by m interacting kink-antikink pairs. In the middle, the behavior is step dependent; the solutions can be complicated, as above, or quasiperiodic with two frequencies, as on the $m = 4$ step. Some of the steps contain substructure, e.g., the $m = 1$ and $m = 2$ steps of Fig. 2.

Finally we turn to the case $M \geq 1$. The whirling solution is given by $\phi_j^*(t) \approx \omega t + 2\pi Mj/N$. To study its linear stability, we substitute this $\phi_j^*(t)$ into (3), use the same Fourier expansion for u_j, and neglect the damping term. The amplitudes satisfy

$$\ddot{A}_m + \omega_m^2 A_m + \varepsilon(e^{i\omega t}A_{m-M} + e^{-i\omega t}A_{m+M}) = 0,$$

where $\varepsilon = 1/2$ is treated formally as a small parameter. This equation is more complicated than (4) because the modes are coupled. Using the method of multiple time scales [14,17,22], we find [19,23] that the onset of instability occurs at

$$\omega \approx \omega_m + \omega_{m+M} \pm \varepsilon(\omega_m\omega_{m+M})^{-1/2}. \qquad (5)$$

Thus the resonances occur at $\omega_m + \omega_{m+M}$, with an $O(\varepsilon)$ correction. As before, the plus (minus) sign corresponds to ω_+ (ω_-). In contrast to $M = 0$, the instabilities arise here from Hopf bifurcations [19]. The slow second frequency is approximately $\varepsilon(\omega_m\omega_{m+M})^{-1/2}$.

We have also measured the onset of instability for $M = 1$ in our Josephson ring. Figure 4 shows that for low voltages a resonant step occurs at $V = 0.75V_0$. As shown in [6], this is the region where the vortex is accelerated up to the speed of light in the system. At $I = 0.35NI_c$, the jump to the gap region occurs. Three resonant steps are visible in the return path, but they now occur at different voltage positions from $M = 0$. The inset of Fig. 4 plots the measured voltages of the resonant steps, along with the prediction of Eq. (5) for $M = 1$. Again, no fitting parameters enter the analysis. There is good agreement between the data and our model.

In numerical simulations for $M = 1$, similar steps are obtained [19]. Their positions are well explained by Eq. (5) and, as predicted, supercritical Hopf bifurcations occur at their onset $\omega = \omega_-$. The dynamics once again become complicated in the middle of a step and simple at the top, where kinks and antikinks are interacting.

The results are qualitatively unchanged for $M > 1$. Resonant steps are observed experimentally, and their locations are explained by our theory. Such agreement for all M suggests that the Josephson rings investigated here are promising model systems for further studies of

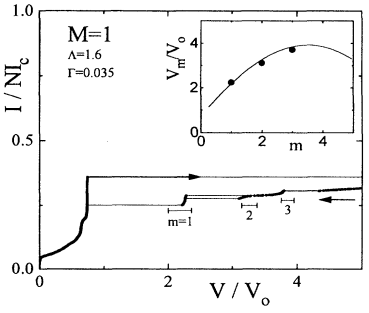

FIG. 4. Experimental I-V curve for $M = 1$. Both axes are normalized. Horizontal bars are instability intervals predicted by (5). Inset: dots, measured voltages of the steps vs mode number m; curve, theoretical estimate $\omega = \omega_m + \omega_{m+M}$ of (5).

the discrete sine-Gordon equation and its spatiotemporal dynamics.

Research supported in part by NSF Grants No. DMR-9402020, No. DMS-9057433, and No. DMS-9111497. We acknowledge the support of AT&T, IBM, and MIT Lincoln Laboratory in the fabrication of the samples.

*Present address: Kimball Hall, Theoretical and Applied Mechanics, Cornell University, Ithaca, NY 14853.

†Present address: Kamerlingh Onnes Laboratory, Leiden University, P.O. Box 9506, 2300 RA Leiden, The Netherlands.

[1] S. H. Strogatz and I. Stewart, Sci. Am. **269**, No. 6, 102 (1993).

[2] P. Hadley *et al.,* Phys. Rev. B **38**, 8712 (1988); K. Wiesenfeld and P. Hadley, Phys. Rev. Lett. **62**, 1335 (1989).

[3] K. Y. Tsang and I. B. Schwartz, Phys. Rev. Lett. **68**, 2265 (1992).

[4] S. Watanabe and S. H. Strogatz, Phys. Rev. Lett. **70**, 2391 (1993); Physica (Amsterdam) **74D**, 197 (1994).

[5] A. V. Ustinov *et al.,* Phys. Rev. B **47**, 8357 (1993).

[6] H. S. J. van der Zant, T. P. Orlando, S. Watanabe, and S. H. Strogatz (to be published).

[7] S. Aubry and L. LeDaeron, Physica (Amsterdam) **8D**, 381 (1983).

[8] M. Levi, Ergod. Th. Dynam. Sys. **8**, 153 (1988); in *Analysis, Et Cetera,* edited by P. Rabinowitz and E. Zehnder (Academic Press, New York, 1990), p. 471.

[9] Y. Imry and L. S. Schulman, J. Appl. Phys. **49**, 749 (1978); E. J. Doedel *et al.,* IEEE Trans. Circ. Syst. **35**, 810 (1988); D. G. Aronson *et al.,* Int. J. Bifurcation Chaos **1**, 51 (1991); M. Henderson *et al.,* Int. J. Bifurcation Chaos **1**, 27 (1991).

[10] K. Maginu, SIAM J. Appl. Math. **43**, 225 (1983).

[11] S. H. Strogatz, *Nonlinear Dynamics and Chaos* (Addison-Wesley, Reading, MA, 1994); M. Levi *et al.,* Quart. Appl. Math., July 1978, 167 (1978).

[12] V is also appropriate notation in the Josephson context, where $V = \langle \dot{\phi} \rangle$ is proportional to the junction *voltage*.

[13] R. Grimshaw, *Nonlinear Ordinary Differential Equations* (Blackwell Scientific Publications, Oxford, 1990).

[14] D. W. Jordan and P. Smith, *Nonlinear Ordinary Differential Equations* (Oxford Univ. Press, Oxford, 1987), 2nd ed.

[15] Maginu [10] has shown that the same parametric instability mechanism occurs in *continuous* Josephson rings; thus it is not a discreteness effect.

[16] The other instabilities with $n > 1$ may be weaker [17].

[17] For a related example, see J. M. Galpin *et al.,* J. Fluid Mech. **239**, 409 (1992).

[18] If the effects of weak damping are included, the leading order approximation to the resonant frequency becomes $\omega \approx 2\omega_m(1 - \Gamma^2/8\omega_m^2)$, valid for $1 \ll \omega_m < 1/\Gamma$. For our arrays, $(\Gamma/\omega_m)^2 < O(10^{-3})$ so the correction due to damping is negligible.

[19] H. S. J. van der Zant, T. P. Orlando, S. Watanabe, and S. H. Strogatz (to be published).

[20] We chose $N = 10$ junctions because the bifurcation sequence along a step is interesting. In our simulations of $N = 8$, no bifurcations occurred after the initial period doubling.

[21] There is no onset for the left end of the $m = 5$ interval since the $m = 4$ mode is already unstable. However, it is not clear whether this can explain the absence of the $m = 5$ step in Fig. 2.

[22] A. H. Nayfeh and D. T. Mook, *Nonlinear Oscillations* (John Wiley & Sons, New York, 1979).

[23] The case $\omega_m = 0$ is exceptional and must be treated separately [19].